JOURNAL OF AIRCRAFT
Vol. 44, No. 3, May–June 2007

Development of a Trailing Vortex Formed with Spanwise Tip Jets

A. G. L. Holloway* and S. Richardson†
University of New Brunswick, Fredericton, New Brunswick E3B 5A3, Canada

DOI: 10.2514/1.25407

Trailing vortices from a NACA0015 ($AR = 5$) wing were formed with spanwise tip jets to allow the study of vortex core distortions on the development of vortex size and speed. The wing-tip jets were formed from small holes arranged along the periphery of the wing cross section. Experiments covered a wide range of tip jet blowing rates for a fixed-wing incidence of 5 deg and chord Reynolds number of 10^5. Measurements of mean velocity, mean vorticity, and turbulence kinetic energy in the wake were made up to 32 chords downwind using hot-wire anemometry. The tip vortex was observed to envelop the jet and subsequently grow in diameter at a substantially higher rate than the vortex formed without tip jets. The circumferential speed of the vortex formed with tip jets was higher in the near field, but declined sharply with downstream distance. At 32 chords downwind, the vortex formed with tip jets evolved into an axisymmetric form similar to a natural vortex, but with a diameter up to three times larger and a peak circumferential velocity three times less. The turbulence intensity measured on the vortex core was 30% in the near wake and 10% at 32 chords downwind.

Nomenclature

AR	=	aspect ratio
b	=	wing span
C_L	=	lift coefficient
C_μ	=	jet-momentum coefficient, $\dot{m}_j V_j / \frac{1}{2}\rho U_\infty^2 S_W$
c	=	wing chord
k	=	kinetic energy of the turbulence, $\frac{1}{2}(\overline{u^2} + \overline{v^2} + \overline{w^2})$
$\dot{m}_j$	=	mass flow rate of the tip jet
q_j	=	volume flow rate of the tip jet
R_c	=	radius of $V_{\theta m}$
Re	=	Reynolds number, $\rho U_\infty c/\mu$
r	=	radial distance from the vortex center
S_w	=	planform area of the wing, bc
$\bar{U}, \bar{V}, \bar{W}$	=	components of the mean velocity along the x, y, and z axes
U_c	=	velocity at the center of the vortex core
U_∞	=	freestream velocity
$\bar{V}_\theta$	=	mean tangential velocity
$V_{\theta m}$	=	maximum tangential velocity
x	=	streamwise coordinate measured from the trailing edge of the wing
y	=	coordinate parallel to wing span
z	=	coordinate in the direction of lift
α	=	angle of wing incidence
Γ	=	circulation
Γ_∞	=	circulation in the freestream
$\bar{\zeta}_x$	=	streamwise component of mean vorticity
θ	=	circumferential position within the vortex core
ν	=	kinematic viscosity
ν_T	=	turbulent viscosity
ρ	=	fluid density

Introduction

THE wing-tip vortex of an airplane can be quite long-lasting, given appropriate initial circulation and lack of interference. In congested airspace, the vortices left by heavier aircraft can adversely affect another aircraft's stability when it is traveling along the same flight path, even minutes later. Currently, air traffic is controlled using standard wait times between aircraft, based on their weights. These times are taken from experimentation and flight tests, because reliable prediction methods do not exist for practical circumstances [1].

In addition to fixed-wing aircraft, rotor performance can suffer from interference with wing-tip vortices. The rotor blades of a helicopter, airplane, or ship propeller produce very strong, concentrated vortices, which can be encountered by the other blades in the rotor set. Interactions between these vortices and the blades, and even the airframe, cause noise and vibrations [2]. Controlling or changing the properties of these vortices could reduce or prevent adverse aerodynamic effects.

A review of existing knowledge on trailing vortex lifespan by Spalart [1] discusses the prediction of vortex dissipation. Two approaches to prediction of the long-term behavior of trailing vortices are considered: the *predictable decay* model in which the kinetic energy of a vortex is gradually dissipated as the vortex is diffused and the *stochastic collapse* model. The mechanism of destruction in the latter model is a crisis caused by internal instabilities, at which time the vortices are greatly deformed and kinetic energy is suddenly dissipated. The crisis may be precipitated by random atmospheric turbulence and deviations from two-dimensional form. The present study considers the effect of vortex core distortion on vortex decay, with changes in streamwise and tangential velocity being produced by spanwise jets on the wing tips.

Analytical Considerations

The simplest vortex models consider a two-dimensional vortex core that has no dependence on the streamwise axial position. The axial velocity is an arbitrary constant. This is often referred to as a two-dimensional line vortex. A laminar model of this vortex will exhibit very slow decay, during which the total circulation is conserved and angular momentum is diffused to larger radii. A description of a two-dimensional laminar vortex is the Lamb–Oseen model [3], which is an exact, but not unique, solution of the Navier–Stokes equations. All streamlines in this model are circular, with vorticity being a function of radial position and time. Saffman [3] describes the development of vorticity using the equation

$$\frac{\mathrm{d}\zeta}{\mathrm{d}t} = \nu\nabla^2\zeta \tag{1}$$

Received 24 May 2006; accepted for publication 22 September 2006.

*Professor, Department of Mechanical Engineering, Box 4400.
†Graduate Student, Department of Mechanical Engineering, Box 4400.

which has the solution

$$\zeta = \frac{\Gamma_\infty}{4\pi\nu t} e^{-\eta} \tag{2}$$

where

$$\eta = \frac{r^2}{4\nu t} \tag{3}$$

is a similarity variable. For an initially concentrated line vortex of Γ_∞, the circulation within r evolves as

$$\Gamma = \Gamma_\infty (1 - e^{-\eta}) \tag{4}$$

Using the definition of circulation $\Gamma = 2\pi V_\theta r$, the tangential velocity development can be derived from Eq. (4) as

$$V_\theta = \frac{\Gamma_\infty}{2\pi r}(1 - e^{-\eta}) \tag{5}$$

The assumption of laminar flow within the core allows only molecular diffusion of vorticity and tangential velocity. The core radius, defined as the position of peak value $V_{\theta m}$, occurs at $\eta_m = 1.25643$. R_c grows as

$$R_c(y) = \sqrt{R_{\text{co}}^2 + 4\eta_m \nu t} \tag{6}$$

where R_{co} is the radius at $t = 0$. A laminar trailing-vortex solution derived by Batchelor [4] expands on the simple line vortex development by coupling the streamwise and circumferential velocities within the vortex using the pressure field. The solution for V_θ in this model is taken to be Eq. (5), under the assumption that radial convection can be neglected (a dubious assumption in the near field). The streamwise gradient of the core pressure is related to the streamwise velocity gradient within the core:

$$\frac{\partial P}{\partial x} \cong U_\infty \frac{\partial U}{\partial x} \tag{7}$$

And the radial gradient of the core pressure is determined by the circumferential velocity:

$$\frac{\partial P}{\partial r} \cong \rho \frac{V_\theta^2}{r} \tag{8}$$

Batchelor [4] thus derived a streamwise velocity development of the form

$$U_\infty - U = \frac{e^{-\eta}}{8\nu x}\left\{\frac{D}{\pi\rho} + \frac{\Gamma_\infty^2}{4\pi^2}\left(1 + \ell_n \frac{x}{b}\frac{\nu}{U_\infty b} + e^\eta Q(\eta)\right)\right\} \tag{9}$$

where the similarity variable is transformed to include streamwise distance, assuming a convection rate U_∞ and $\eta = U_\infty r^2/4\nu x$. The parameter D is the total drag on the wing, and $Q(\eta)$ is a function that is zero at the center and edge of the vortex and has a maximum value of 0.13. Equation (9) always predicts a surplus at small x (a value dependent on the circulation and drag), which decays as $\sim x^{-2}$. However, it also predicts that a streamwise velocity deficit ultimately develops on the core and this decays as $\sim x^{-1}\,\ell_n(x)$ in the far wake. The physical explanation of this behavior is that when the tangential velocity decreases, the core pressure rises, resulting in a deceleration of the core streamwise flow. The velocity deficit never achieves a decay rate typical of a laminar axisymmetric wake without swirl $\sim x^{-1}$. Equation (9) does not explicitly account for the flow of energy of the tip jets used in the present study. The simplest aerodynamic model of these jets would be a source for which the contribution to the streamwise velocity would be $u = q_j/4\pi x$ and to the drag would be $-\rho U_\infty q_j$, which would count as a thrust. Of course, for any isolated body, such as an airplane, the source must be balanced by a sink elsewhere in the flow.

Under what circumstances the streamwise velocity on the natural vortex core exceeds the freestream velocity has also been addressed by Brown [5], who calculated an axial velocity distribution expected to be valid in the very near wake before much diffusion has taken place. In his description, the induced drag results from the vortex sheet roll up and is responsible for a low pressure on the core and, hence, higher core velocity. The profile drag results from slow boundary-layer material leaving the wing and, hence, contributes to a lower core velocity. The formula given is

$$U_\infty - U = \left\{\frac{3}{2bU_\infty}\right\}\left\{\frac{D_P}{2\pi\rho} - \frac{\Gamma_\infty^2}{4\pi^2}\right\}\frac{1}{r} \tag{10}$$

where D_P is the parasitic drag for the whole wing. No friction within the vortex is accounted for and therefore the velocity at the center is undefined. Brown [5] also predicts that in the far wake, $R_c \sim x^{2/3}$. The case of a velocity deficit on the natural vortex core is evident in the current study and in those of Devenport et al. [6] and of Heyes and Smith [7]. The data from Simpson et al. show a velocity surplus on the core of the natural vortex. Equation (10) suggests that this indicates a high ratio of induced drag to profile drag in that case.

In a simple line vortex, such as that described by Saffman [3], stability can be proven for $\mathrm{d}\Gamma^2/\mathrm{d}r > 0$. Furthermore, Uberoi [9] hypothesizes that instability in a line vortex must be caused by axisymmetric swirl flows within the vortex core having $\mathrm{d}\Gamma^2/\mathrm{d}r < 0$. Swirls do not contribute to the freestream circulation. In the case of the trailing vortex, a deficit or surplus of streamwise velocity on the vortex core can also produce flow instability similar to that of an axisymmetric jet or wake.

There is some evidence that the vortex core is laminar, but that this region is surrounded by a layer of turbulent fluid, the origin of which is uncertain. Squire [10] proposed a simple model of turbulent vortex diffusion using a uniform turbulent viscosity $\nu_T \sim \Gamma_\infty$. Because ν_T is a constant across the vortex, the mean circumferential velocity would take the form of Eq. (5) and the core radius would grow as $R_c \sim (\Gamma_\infty x/U_\infty)^{0.5}$. Alternatively, Uberoi [9] proposed a similarity solution of the turbulent vortex problem that does not assume a uniform value of the turbulent viscosity:

$$\frac{\Gamma}{\Gamma_\infty} = 1 - [1 + 15(e^{10\eta} - 1)]^{-1} \tag{11}$$

where $\eta = r^2 U_\infty/\Gamma_\infty x$. The predicted growth of the vortex core is essentially the same as Squire's model.

Literature Review

There are many published studies on the anatomy and development of the natural wing-tip vortex (no tip jets) and the study by Devenport et al. [6] is very closely related to the present work. It includes wake measurements for a NACA 0012 half wing made with hot-wire anemometry in cross-stream planes between 5 and 30 chords downwind. Results showed an almost laminar vortex core after correction for wandering motions. Outside of the core they found that a turbulent spiral was the dominant feature of the vortex wake. The vortex development up to 30 chords showed only small changes in the core radius, peak tangential velocity, and axial velocity deficit. This study did not investigate the destruction or dissipation of trailing vortices by artificial means.

Studies of spanwise blowing from the tip of a lifting wing are less known but they have a long history. The first recorded research activity on using spanwise blowing to improve wing performance was in 1956, by Ayers and Wilde [11]. A few other small studies in the following 25 years touched the wing-tip blowing subject, but in the 1980s, comprehensive studies at the University of Tennessee [12–17] and Stanford University [11–26] were done. In 2000, research into tip blowing was initiated at the University of New Brunswick [27].

A rectangular NACA 0012 wing with spanwise jets on the wing tip was used by Wu et al. [16] to compare the effectiveness of spanwise blowing to passive winglets. Results were positive as the pressure across the top surface of the wing was lowered, whereas the pressure on the bottom stayed the same as without blowing. A flow visualization study of wing-tip blowing using a water tunnel was also done [18], using the same shape of wing but with lower Reynolds

numbers (10^4) to allow visualization of the vortex. This study showed important effects of wing-tip blowing on vortex behavior, such as an increased dispersion of the wake and vortex, an outward shift of the vortex core, and contra-rotating vortices typical of a jet in crossflow. The study defined a nondimensional jet-momentum coefficient to represent the degree of tip blowing:

$$C_\mu = \frac{\dot{m}_j V_j}{\frac{1}{2}\rho U_\infty^2 S_w} \tag{12}$$

Tavella et al. [23,24] investigated the general effect of wing-tip blowing on a rectangular wing of a NACA 0018 cross section with a wing-tip blowing slot running most of the length of the chord. Several angles of attack and blowing rates were used. The pressure distributions that resulted showed a universal decrease in the top surface pressure and a gain of pressure on the lower surface, which is consistent with the finding of Wu et al. [16]. The positive results on the lift increment $\Delta C_L/C_{L_o}$, where C_{L_o} is the lift coefficient without blowing, indicate that effects were most significant for low aspect ratio. In addition to the lifting force studies, Lee et al. [19] measured the cross-stream velocities 1.4 chords behind the trailing edge of the wing. They showed that the vortex was outwardly displaced and upwashed by blowing.

A study by Jeans [27], at the University of New Brunswick, measured the effects of wing-tip blowing using a NACA 0015 half wing with $AR = 5$, the same wing apparatus as in the current study. Increments of lift measured with tip jet blowing were consistent with previous studies. Some of the results have been plotted along with inviscid theory for comparison in Figs. 1 and 2. A high blowing rate, higher than practical for aircraft applications, has been chosen to clearly demonstrate the effects. The pressure data match well to rectangular wing theory in the nonblown case and to 2-D wing theory for the case using spanwise tip jets. The effect of the jets is greatest near the tip and occurs mostly on the upper surface.

Subsequently, this apparatus was used for a wake study by Bettle [28] that included mean flow and turbulence quantities. This study focused on the near wake with objectives of gaining better understanding of the general effects of tip blowing and the effects of wing-tip clearance in the presence of tip blowing. Hot-wire anemometry was used to survey the wake up to four chords downstream of the wing. Figure 3 shows the mean velocity measurements taken at one chord downwind. The tip vortex and jet fluid rolled up to produce a larger vortex with clockwise and counterclockwise rotation and a core axial velocity surplus. At $x/c = 1$, the same surplus in streamwise velocity was observed for angles of wing incidence $\alpha = 0$, 5, and 10 deg.

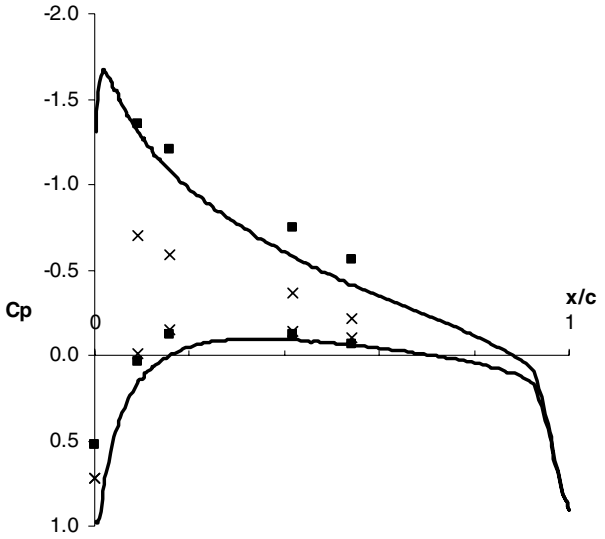

Fig. 1 Pressure distribution at 96% of the wing span [27]. Experimental conditions were $\alpha = 5$ deg, $C\mu = 0$ (×), and $C_\mu = 0.28$ (■). The solid line is from 2-D airfoil theory.

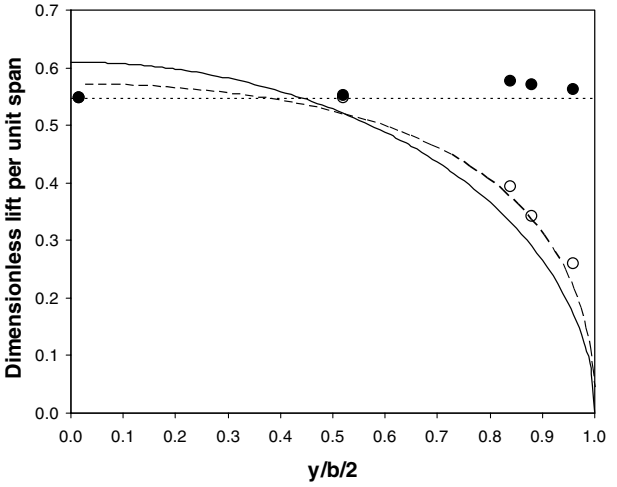

Fig. 2 Loading along the wing span [27]. Experimental conditions were $\alpha = 5$ deg and $C_\mu = 0.28$ for the blowing case.

The primary findings of Bettle [28] included the dispersion and outward movement of the vortex, consistent with earlier studies, along with high kinetic energy of turbulence and excess core momentum. The advantageous effects of tip jets on the lift coefficient were found to also occur with reduced tip clearances, albeit at lower values of C_μ. At very small tip clearances, the lift coefficient was diminished by tip blowing.

The study by Simpson et al. [8] investigated the effects of straight and Coanda-type tip jets on the near wake of a lifting wing. A rectangular wing with a NACA 0015 profile was used. The wing tip was rounded, and the tip jet was situated at one-quarter chord back of the leading edge. Hot-wire surveys of the wake were done at $x/c = 1.67$, $\alpha = 10$ deg, and $C_\mu = 0.065$. Findings included a 55% reduction in maximum tangential velocity when using tip jets compared with the natural vortex and an increase of vortex diameter of 2.5 times at $x/c = 1.67$ downstream. Only a slight difference was found in the results between the straight and Coanda-type jets. The natural vortex was also measured as a baseline in this study, and the core axial velocity was found to be higher than the freestream velocity by about 40%. The spanwise tip jets caused the axial velocity to form a deficit on the core of about 20%.

The study by Heyes and Smith [7] compared the near wake velocity field with and without steady spanwise tip jets and with

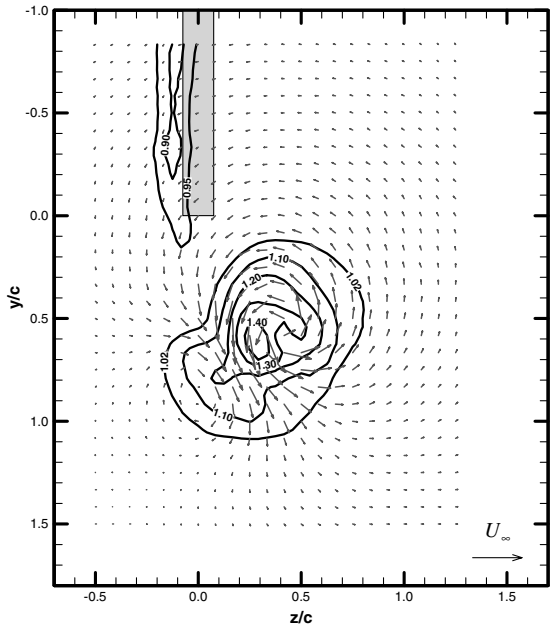

Fig. 3 Streamwise velocity contours $\bar{U}/U_\infty$ and cross-stream vectors [28]. Measured at $x/c = 1$ with $\alpha = 5$ deg and $C_\mu = 0.28$.

pulsed tip jets. Particle image velocimetry and hot-wire measurement techniques were used to measure the wake velocity. The wing was a NACA 0012 ($AR = 2$) with rectangular planform, chord Reynolds number of 2.2×10^5, $C_\mu = 0.015$, and $\alpha = 7.5$ deg. Different wing tips were used with varying geometries, but the air always exited parallel to the wing span. The natural vortex measured in this study showed a core axial velocity deficit of ~10%. Of particular interest to the current study were the results using steady blowing, which showed an increased deficit of core axial velocity with the use of spanwise tip jets over the nonjet case. The near wake measurements ($x/c = 1$) also showed reduction of the tangential velocity for all jet-momentum coefficients and increased growth proportional to the blowing rate.

The study by Han and Leishman [2] investigated the use of tip jets to modify the tip vortex generated by a rotor blade. In this study, a model wing was made with internal passages running from the leading edge to tip of the blade. The total pressure difference between the entrance and exits of each passage results from the centrifugal action of the spinning blade and produces a flow exiting from the wing tip, adding to the vortex fluid. It was reported that the maximum swirling velocities were reduced by as much as 60% and diffusion was up to three times faster. The Squire model [10] adapted to the rotor blade geometry

$$R_c = \sqrt{R_{c0}^2 + 4\eta_m \nu_T \zeta/\Omega} \tag{13}$$

was used to model the vortex diffusion. The rotor rotational speed is Ω, and ζ is the wake age in degrees. A turbulent eddy viscosity to viscosity ratio (ν_T/ν) was found equal to about 8 without tip blowing and as high as 16 with tip blowing.

One of the near-field features of the present flow is an axial velocity surplus and counter-rotating vortices. This can perhaps be best understood by recognizing them as features of a jet in crossflow. Studies by Findlay et al. [29], Crabb et al. [30], and Andreopoulos and Rodi [31] measured the wakes of jets in crossflow with varying velocity ratios (jet to cross stream) and jet exit geometries. The jet is subjected to a drag force from the freestream crossflow that results in its bending downwind and the production of two counter-rotating vortices of equal and opposite strength within the jet material. A result found in studies for which jet velocities exceeded the freestream velocity was that the jet speed was maintained while being turned. That is, in the near field, the streamwise velocity on the jet axis was above that of the freestream in spite of the fact that it initially had no streamwise momentum. These are similar features to the present study. In the far field, the jet diffuses and velocities tend toward the freestream speed.

None of the previous studies cited here have considered the ultimate downstream shape and scale of the vortex formed with tip blowing. The purpose of the present study is to address this by performing measurements of mean velocity and turbulence up to 32 chords.

Experimental Apparatus

All experiments described in this paper were performed in the wind tunnel at the University of New Brunswick. It is an open-return system with a mixed flow fan powered by a variable-speed 20-hp drive. The tunnel has a large settling chamber and a 16:1 contraction attached to a square 5-m-long test section having a cross section of 58 cm^2. The contraction produces a near uniform flow with a turbulence intensity $u'/U < 0.1\%$ and maximum flow speed of 27 m/s. A schematic of the test section with the wing and instrumentation is shown in Fig. 4.

The probe positioning in any streamwise plane is controlled by stepper motors with a precision of ± 0.1 mm. The streamwise position was adjusted manually to ± 1 mm. The probe positioning mechanism was shaped to reduce its effect on the flow.

The wing was machined to a NACA 0015 profile, but with small spanwise grooves to promote turbulence. It was suspended from the tunnel roof and its angle of attack was adjusted manually or with a computer-controlled stepper motor. The wing had a half span (from tunnel roof to tip of wing) of 30 cm and a chord of 12 cm. At the tip of the wing were 50 1-mm holes though which air was forced to generate a sheet of spanwise jets, shown in Fig. 5. It is the same wing used by Jeans [27], and Bettle [28].

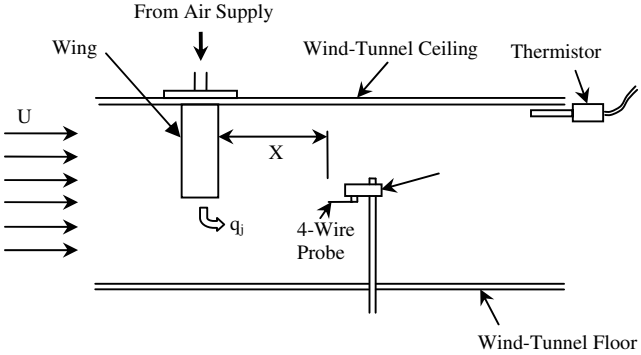

Fig. 4 Wind tunnel and experimental setup.

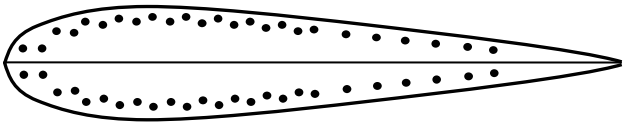

Fig. 5 Wing-tip configuration.

The pressurized air used for the tip jets was drawn from a 450-liter compressed air tank located in the laboratory. The tank was large enough to ensure a constant flow rate and temperature. The flow rate of air through the jets was monitored using a continuous flow meter in the flow supply line. The geometric angle of incidence of the wing used in the present study was 4.8 deg, with a correction [32] based on the tunnel geometry of $\Delta\alpha \sim 0.5$ deg.

Instrumentation

Velocity measurements were made with an Auspex Corp. four-wire thermal anemometer probe that allowed simultaneously measurement of three velocity components. This was found necessary in this strongly three-dimensional vortex flow.

The wire configuration of the probe is sketched in Fig. 6. Four center prongs extend out from the main probe body and from each a wire is strung back at an angle of nominally 45 deg to its outer prong. Devenport et al. [6] used an alternate four wire configuration and concluded that four wire probes were better than standard triple and X-array probes for trailing vortex measurement, because they are less sensitive to streamwise vorticity.

Calibration of the hot-wire probe was based on the assumption that speed and directional effects are independent. Speed calibrations were done in-situ before and after measurement runs to generate calibration curves for each wire. This calibration data were fit to King's law:

$$\frac{E^2}{T_{\text{wire}} - T_\infty} = A + BU^{0.45} \tag{14}$$

where E is the anemometer voltage, U is the wind-tunnel speed, and A and B are calibration constants. The air temperature T_∞ was taken

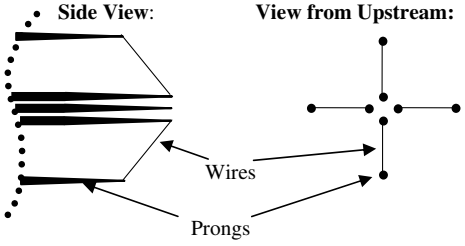

Fig. 6 Four-wire probe and wire configuration.

at the time of calibration and replaced with the air temperature measured by a thermistor mounted in the airstream. T_{wire} was kept constant, with the anemometer bridge at 200°C above the ambient temperature, corresponding to an overheat ratio of 1.72.

Directional calibration was done in two steps. The first was based on the assumption that the effective cooling velocity is equal to the component normal to the wire's length and that opposing pairs of wire may be treated separately without correction for cooling due to out-of-plane and longitudinal velocities. The effective cooling velocities can then be related to the instantaneous velocity components [28] U, V, and W as

$$\begin{aligned} V_0 &= U\cos\alpha_0 + V\sin\alpha_0 \qquad V_1 = U\cos\alpha_1 - V\sin\alpha_1 \\ V_2 &= U\cos\alpha_2 - W\sin\alpha_2 \qquad V_3 = U\cos\alpha_3 - W\sin\alpha_3 \end{aligned} \tag{15}$$

The angles α_0, α_1, α_2, and α_3 are the thermally effective wire angles that were measured to be approximately 37 deg from the probe axis. For data processing, Eqs. (15) are rearranged to solve directly for the instantaneous velocity components U_1, U_2, V, and W. The redundancy in the streamwise velocity was resolved by choosing the smaller of the two values. This simple approach required smaller corrections than several more complex alternatives.

The second step of directional calibration is to correct the values from Eq. (15), termed the *apparent velocities*, based on a direct calibration over a range of pitch and yaw covering ±50 deg. This calibration was done in specially made gimbals that held the probe in an air jet of controlled speed. When processing data, a computer program calculates the apparent pitch and yaw from the wire voltage data and then interpolates the actual pitch, yaw, and speed from a database of corrections. The relationship between apparent and actual values is shown in Figs. 7–9. No iteration is required in this process.

Data acquisition was done with a 16-bit data acquisition board and connector accessory. Data inputs were the four anemometers, the pressure transducers used to monitor wind-tunnel speed and tip jet blowing rate, and the thermistor for air temperature monitoring.

Sampling was done at a rate of 1 kHz. It was determined that 50 sets of 2048 samples at each measuring position were adequate for statistical estimates of the mean flow and turbulence level. Each data sampling point amounts to a 10.4-MB file, which translates into 3.5 GB of data for one cross-sectional plane. Probe positioning was fully automated.

The instantaneous velocities were decomposed into mean and turbulent fluctuations. The mean and variance were calculated from

$$\bar{U} = \frac{1}{N}\sum_{i=1}^{N} U_i \tag{16}$$

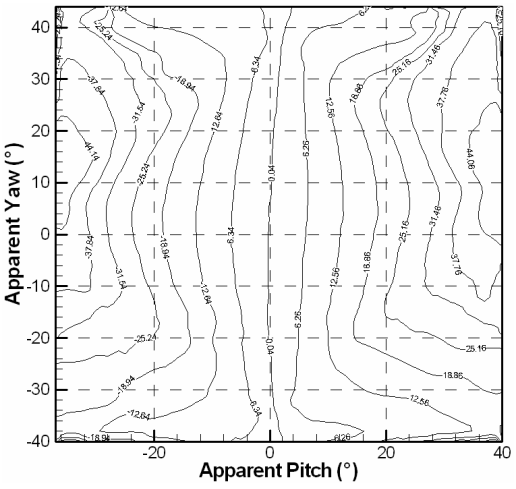

Fig. 7 Actual pitch angle of the velocity vector as a function of apparent pitch and yaw.

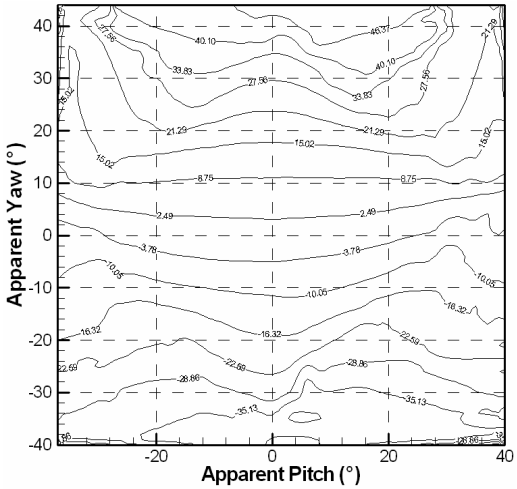

Fig. 8 Actual yaw angle of the velocity vector as a function of apparent pitch and yaw.

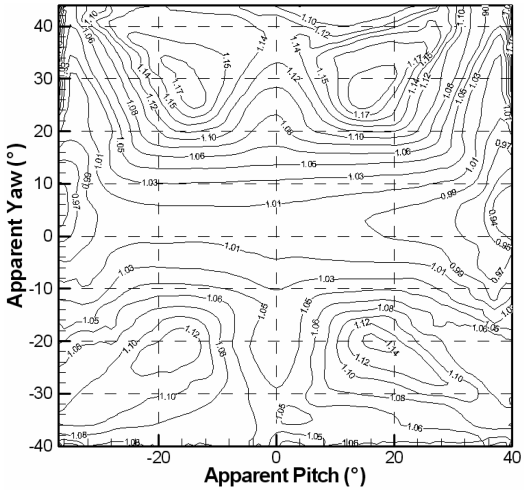

Fig. 9 Velocity magnitude correction as a function of apparent pitch and yaw.

$$\overline{u^2} = \frac{1}{N}\sum_{i=1}^{N}(U_i - \bar{U}_i)^2 \tag{17}$$

The six independent components of the velocity variance form the Reynolds stresses tensor:

$$\sigma_{ij} = \begin{bmatrix} \overline{u^2} & \overline{uv} & \overline{uw} \\ \overline{uv} & \overline{v^2} & \overline{vw} \\ \overline{uw} & \overline{vw} & \overline{w^2} \end{bmatrix} \tag{18}$$

The sum of the diagonal components constitutes twice the turbulence kinetic energy per unit mass, calculated as

$$k = \tfrac{1}{2}(\overline{u^2} + \overline{v^2} + \overline{w^2}) \tag{19}$$

Wind-tunnel studies of vortices, particularly those that attempt measurement at large distances downstream of a lifting wing, encounter vortex wandering. This effect is seen in the velocity data as a random, low-frequency cross-stream motion of the vortex. Devenport et al. [6] gives particular attention to wandering and corrects for it in his measurement of the vortex velocity field. He showed that wandering spatially smeared the measurements of mean velocity and enhanced the velocity variance. It does not constitute turbulence. To help identify the contributions of vortex wandering to the velocity time series they were analyzed using the fast Fourier transform (FFT). Analysis was done for three different cases: in the core of the natural vortex, a point outside the vortex in the freestream,

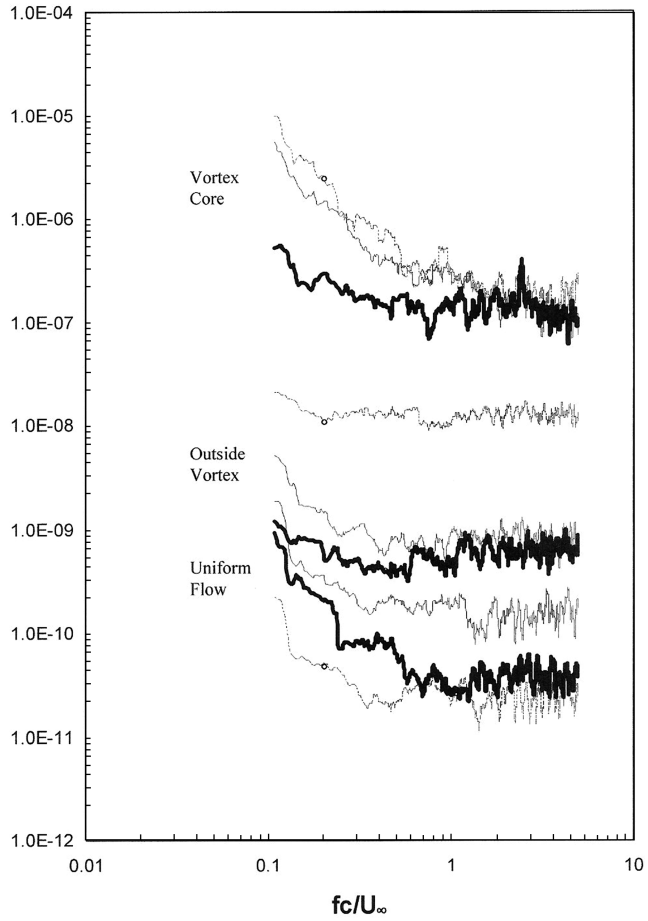

Fig. 10 Comparison of velocity spectra from inside and outside the vortex at $x/c = 8$ (thick line, F_{uu}/U_∞^2; dashed line, F_{vv}/U_∞^2; solid line, F_{ww}/U_∞^2). No wing-tip jets are used.

and in the wind-tunnel freestream with the wing removed. All measurements were taken at the same streamwise position; in the first two cases, this was eight chords downwind of the wing. Spectra of all three components of the velocity are shown in Fig. 10 for each case listed previously. Outside the vortex core, where the motions are largely irrotational, the spanwise spectra is much larger than the other two components. Inside the vortex core, the energy is much greater and the transverse and spanwise motions dominate for $fc/U_\infty < 1$. At higher frequencies, all three components of the spectra are of comparable magnitude. One might conclude that vortex wandering evident in the freestream is responsible for generating the large low-frequency fluctuations that appear in the time series from the core. A notable feature in the high-frequency range is a peak at $fc/U_\infty \cong 2$ (or $ft/U_\infty \cong 0.3$, where t is the thickness of the wing). The effects of wandering will be discussed further in a later section; however, unless specifically stated, no corrections for wandering have been made to the data presented.

Estimation of the mean streamwise component of the vorticity was based on our velocity data array:

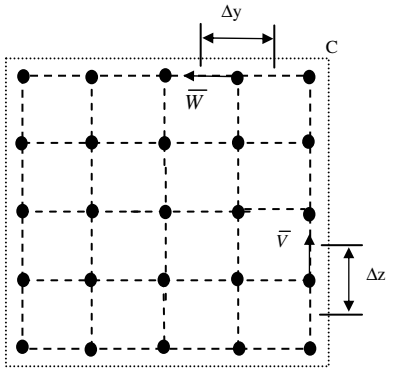

Fig. 11 Line integral for calculation of total circulation.

$$\bar{\zeta}_x \cong \left(\frac{\Delta\bar{W}}{\Delta y} - \frac{\Delta\bar{V}}{\Delta z}\right) \tag{20}$$

where Δy and Δz are the cross-stream spacings of the measurement grid and $\Delta\bar{V}$ and $\Delta\bar{W}$ are the differences in the velocity components across their corresponding grid spacing (see Fig. 11).

The circulation was estimated by using an approximate line integral in which the velocity tangential to the loop C is summed around the loop. The outer edge of the measurement region was chosen to be as large as possible without including the boundary layer on the wind-tunnel walls. The calculation is

$$\Gamma_x \cong \sum_i (\Delta\bar{V}_i \Delta z_i + \Delta\bar{W}_i \Delta y_i) \tag{21}$$

Results

Tests were done for four levels of tip jet flow, eight different streamwise distances, a fixed-wing incidence angle of 5 deg, and a wind speed of 12 m/s. The 54 different measurement conditions are summarized in Table 1. The range of test conditions was chosen to permit a comprehensive evaluation of the effects of tip jet blowing, but it should be born in mind that the higher values of C_μ listed in Table 1 are impractical for full-size aircraft because of the excessive blowing rates that would correspond to their large size and high speed.

Near Wake

The mean velocity, mean vorticity, and kinetic energy of turbulence formed in the near wake ($x/c = 0.5$) without the use of spanwise jets are shown in Figs. 12–14. There are velocity deficits of approximately 10% in the wake of the wing and on the vortex core. Vorticity is concentrated mostly around the vortex, and the highest turbulence is in the wake of the wing, with less turbulence in the vicinity of the vortex core.

Figures 15–17 correspond to $C_\mu = 0.05$. At this blowing rate, the effect of the tip jets is apparent at $x/c = 0.5$. The vortex core has been displaced outward and upward in the direction of lift. The vortex core velocity deficit is small and there are positive and negative lobes of vorticity having unequal strength. Turbulence levels on the vortex core have increased dramatically compared with the natural vortex.

Table 1 Matrix of experimental conditions

Grid spacing	Streamwise positions, x/c	Jet reservoir pressure, kPa	Jet mass flow rate, kg/s	Jet-momentum coefficient C_μ
1 cm^2	0.5, 1, 2, 4, 8, 16, 24, 32	0	0.0	0.0
		6.2	0.0027	0.05
		12.4	0.0038	0.1
.025 cm^2	0.5, 1, 2, 4, 8, 16, 24, 32	0	0.0	0.0
		6.2	0.0027	0.05
		12.4	0.0038	0.1
Hybrid Grid	0.5, 1, 2, 4, 8, 16	45	0.0064	0.28

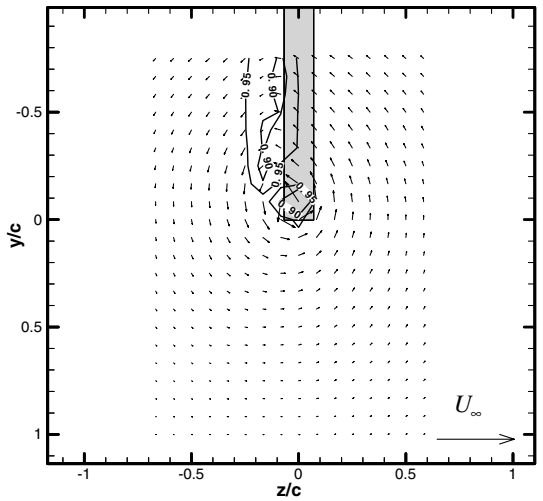

Fig. 12 Streamwise velocity contours $\bar{U}/U_\infty$ and transverse velocity vectors measured at $x/c = 0.5$ for $\alpha = 5\,\mathrm{deg}$ and $C_\mu = 0.0$. The shaded area is the wing silhouette.

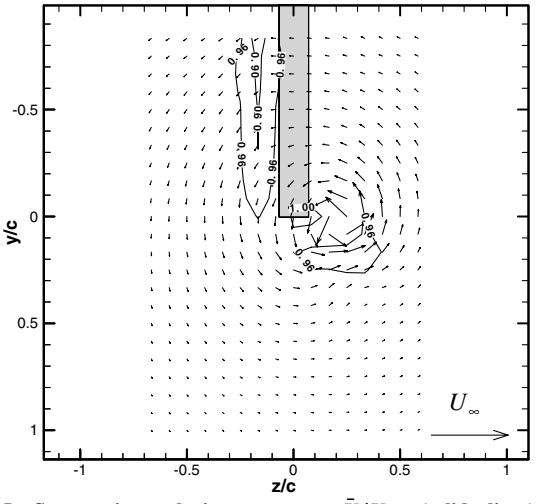

Fig. 15 Streamwise velocity contours $\bar{U}/U_\infty$ (solid lines) and transverse velocity vectors measured at $x/c = 0.5$ for $\alpha = 5\,\mathrm{deg}$ and $C_\mu = 0.05$.

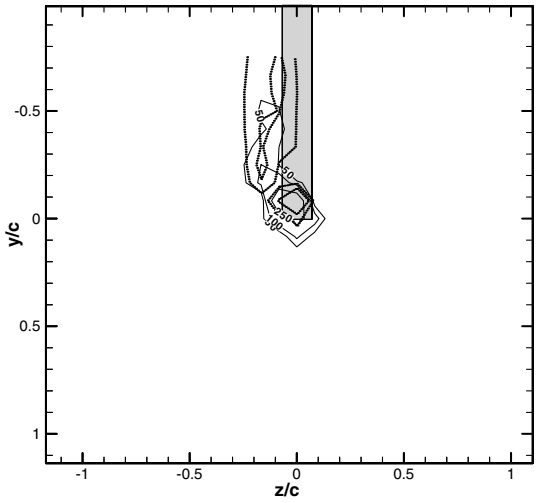

Fig. 13 Vorticity contours ζ_x [s^{-1}] (solid lines) and streamwise velocity contours $\bar{U}/U_\infty$ (dotted lines). Measurements at $x/c = 0.5$ for $\alpha = 5\,\mathrm{deg}$ and $C_\mu = 0.0$.

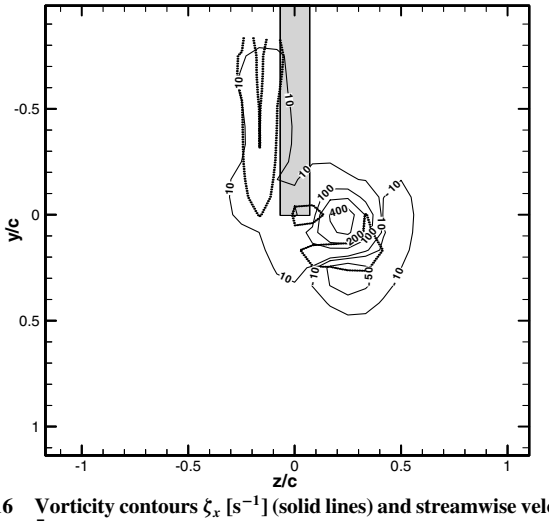

Fig. 16 Vorticity contours ζ_x [s^{-1}] (solid lines) and streamwise velocity contours $\bar{U}/U_\infty$ (dotted lines). Measurements at $x/c = 0.5$ for $\alpha = 5\,\mathrm{deg}$ and $C_\mu = 0.05$.

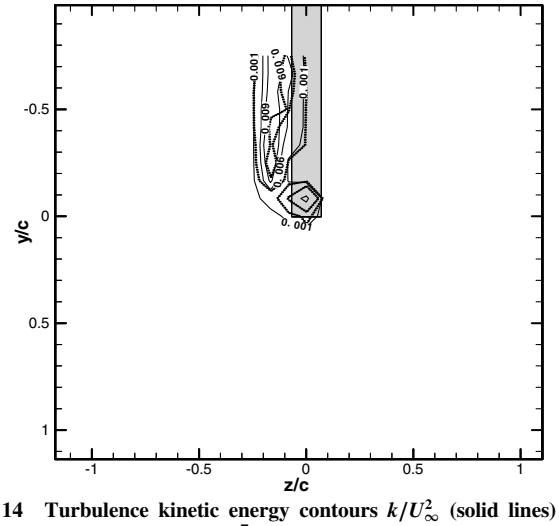

Fig. 14 Turbulence kinetic energy contours k/U_∞^2 (solid lines) and streamwise velocity contours $\bar{U}/U_\infty$ (dotted lines). Measurements at $x/c = 0.5$ for $\alpha = 5\,\mathrm{deg}$ and $C_\mu = 0.0$.

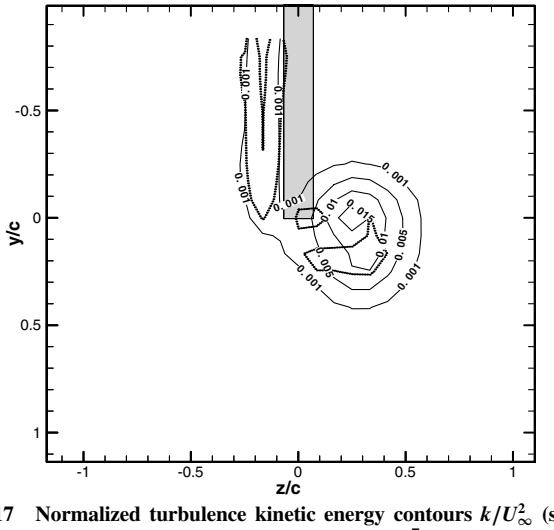

Fig. 17 Normalized turbulence kinetic energy contours k/U_∞^2 (solid lines) and normalized streamwise velocity contours $\bar{U}/U_\infty$ (dotted lines). Measurements at $x/c = 0.5$ for $\alpha = 5\,\mathrm{deg}$ and $C_\mu = 0.05$.

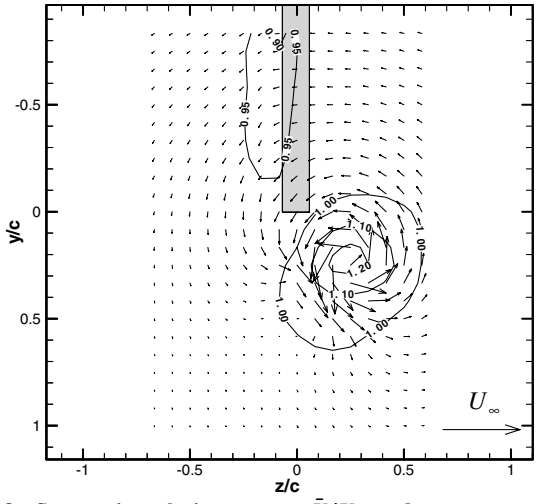

Fig. 18 Streamwise velocity contours $\bar{U}/U_\infty$ and transverse velocity vectors measured at $x/c = 0.5$ for $\alpha = 5$ degand $C_\mu = 0.1$.

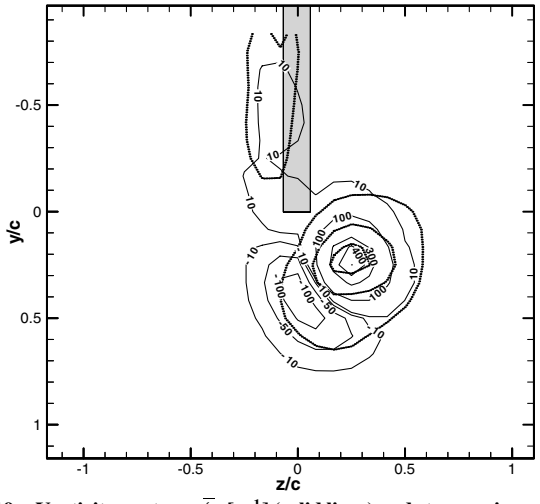

Fig. 19 Vorticity contours $\bar{\zeta}_x$ [s^{-1}] (solid lines) and streamwise velocity contours $\bar{U}/U_\infty$ (dotted lines). Measurements at $x/c = 0.5$ for $\alpha = 5$ deg and $C_\mu = 0.1$.

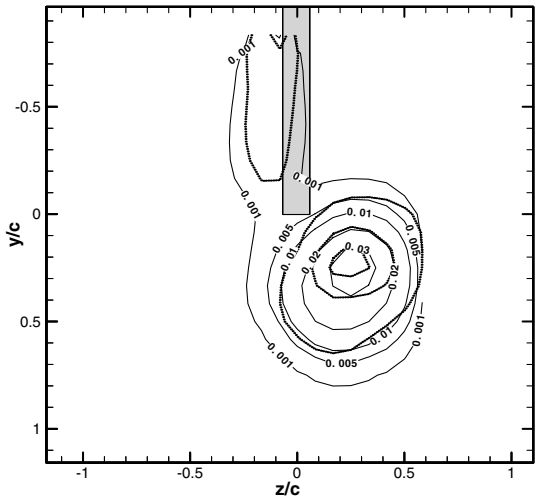

Fig. 20 Turbulence kinetic energy contours k/U_∞^2 (solid lines) and normalized streamwise velocity contours $\bar{U}/U_\infty$ (dotted lines). Measurements at $x/c = 0.5$ for $\alpha = 5$ deg and $C_\mu = 0.1$.

Results for $C_\mu = 0.1$ are shown in Figs. 18–20. The effects of blowing are similar to that for $C_\mu = 0.05$, yet are more pronounced. The core velocity deficit has now become a surplus of about 20% over the freestream value. The maximum vorticity has not increased significantly over the $C_\mu = 0.05$ case, but the region of negative vorticity is larger and stronger and repositioned. With this doubling of the tip jet momentum, the turbulence on the core has doubled with respect to the $C_\mu = 0.1$ case.

Growth and Development of Vortex Scales

The circulation was calculated from the data in each measurement plane using perimeter velocity measurements; the results are shown in Fig. 21. In each case, the calculated circulation decreases sharply over the first few chords before rising gradually toward $\Gamma \sim 0.3$ m^2/s. The tip jet blowing did not have a significant effect on the freestream circulation. This may seem paradoxical, because the wing lift is observed to increase with tip jet momentum. However, as shown in Fig. 2, this increase in lift comes primarily from a change in the load distribution near the tips and not due to an increase in the

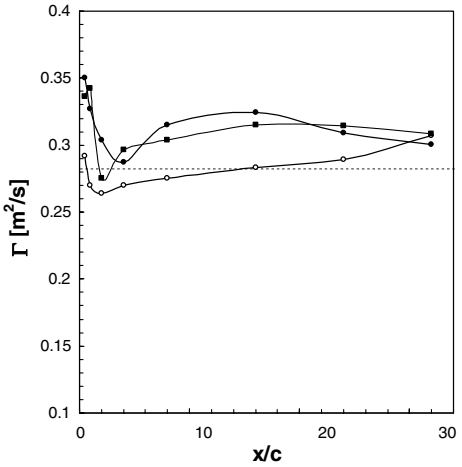

Fig. 21 Streamwise development of the measured freestream circulation. The dotted line represents circulation calculated from finite wing theory. Symbols indicate $C_\mu = 0.0$ (○), 0.05 (■), and 0.1 (●).

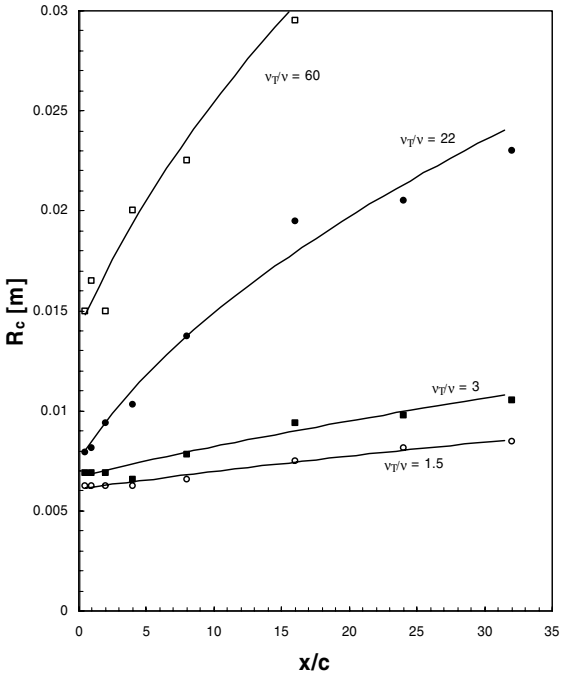

Fig. 22 Streamwise development of the core radius. Symbols indicate $C_\mu = 0.0$ (○), 0.05 (■), 0.1 (●), and 0.28 (□). Solid lines are calculated from Eq. (6), using a turbulent viscosity fit to the data.

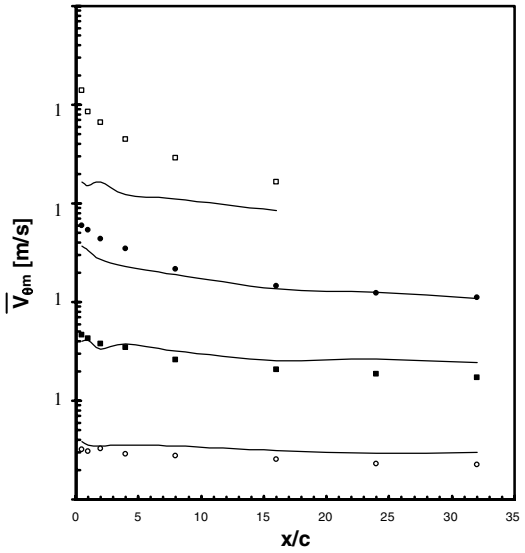

Fig. 23 Streamwise development of the maximum tangential velocity of the vortex core. Symbols indicate $C_\mu = 0.0$ (○), 0.05 (■), 0.1 (●), and 0.28 (□). Solid lines are based on Eq. (11).

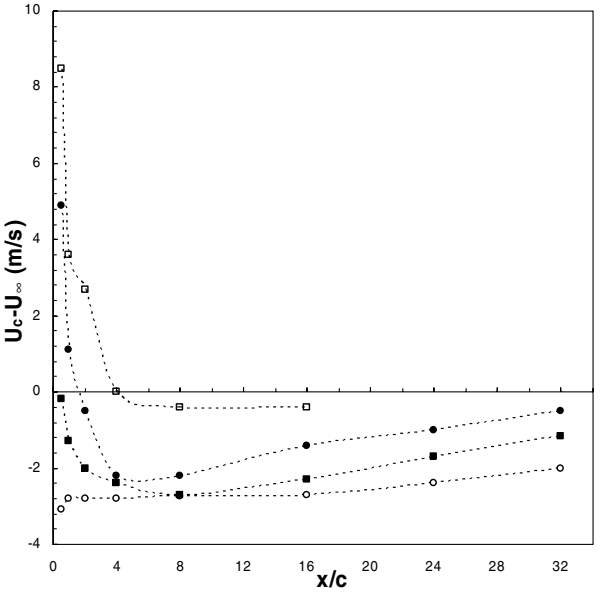

Fig. 24 Development of the streamwise velocity on the vortex core. Symbols indicate $C_\mu = 0.0$ (○), 0.05 (■), 0.1 (●), and 0.28 (□).

maximum bound circulation. It might be expected that for each experimental case (i.e., each jet-momentum coefficient) that the calculated circulation would be constant along the development; however, Fig. 21 shows a slow rise in circulation. This may be due to vorticity shed from across the span of the wing gradually entering the measurement region.

The development of the core radius for each value of C_μ is plotted in Fig. 22. These are average values based on four equally spaced radial profiles taken through the vortex core. The effect of tip jets on vortex growth is clearly demonstrated. Initial vortex size is roughly proportional to the jet-momentum coefficient but the subsequent growth rate is not. For example, the $C_\mu = 0.05$ case has a growth rate similar to the natural vortex, whereas the growth rate for the $C_\mu = 0.1$ case is much more substantial. The solid line represents Eq. (6) with an initial radius size and a turbulent eddy viscosity ν_T/ν, fit to the data in each case. A significant finding is that $\nu_T/\nu = 1.5$ for the natural vortex, which suggests that what random motions are present are not very active in the spread of the vorticity.

The streamwise development of the average value of maximum tangential velocity corresponding to the values of R_c plotted in Fig. 22 is shown in Fig. 23. The solid lines were calculated from Eq. (11) using data for Γ_∞ and R_c from Figs. 21 and 22. Note that the curves have each been shifted by one decade. Although the tip jets generate an initially higher value of $V_{\theta m}$, this declines sharply with downwind distance and, at the end of the measurement region, $V_{\theta m}$ is lower in all cases using spanwise tip jets compared with the natural vortex. Ultimately, all the tangential velocities must decay $\sim x^{-1/2}$ once similarity has been achieved, because the freestream circulation is fixed and the core radius is growing as $\sim x^{1/2}$. A measure of how far the vortices are from similarity is the difference between the data and the line based on Eq. (11).

Another developmental feature of the flow is the axial velocity on the vortex core, shown in Fig. 24. The natural vortex begins with a streamwise velocity deficit on the core, whereas with spanwise tip jets, the core velocity is initially in excess of the freestream. This core velocity surplus steeply declines, becoming a deficit, then the deficit gradually decays in the far wake. This development is qualitatively similar to that described by Eq. (9), but the measured minimum is substantially lower. The rate of deficit decay beyond $x/c = 16$ depends on the blowing rate and cannot be fit by either $x^{-2/3}$ (from turbulent wake similarity) or $x^{-1}\,\ell_n(x)$, which, incidentally, are indistinguishable within the measurement range.

The level of turbulence kinetic energy on the vortex core is plotted vs streamwise distance from the trailing edge of the wing in Fig. 25. In comparison with the natural vortex, wing-tip blowing produced initial values of turbulence that were tenfold higher than that in the natural vortex. In fact, these initial turbulence levels are at or beyond what can be accurately measured with hot-wire anemometry and are best regarded as qualitative. As the flow develops, a decline in the core turbulence level is seen throughout; and at 32 chords, the turbulence levels for all three blowing rates are rapidly converging to that of the natural vortex. This rapid decay of the turbulence level is coincident with the rapid growth of the vortex core and consequent reduction in the mean velocity gradients. High-pass filtering the data at $x/c = 32$ to 10 Hz reduced k/U_∞^2 by approximately 0.003 for all blowing rates.

The mean motion of the vortex core in the wind-tunnel cross section is shown in Fig. 26. The trajectories of the vortex cores that were subjected to varying levels of spanwise tip blowing all exhibited an outward and upward (in the direction of lift) initial motion of the vortex core, followed by a return to the wing silhouette. The $C_\mu = 0.28$ curve is still moving in the direction of lift at the last point of measurement. These motions of the vortex cores are believed to be influenced by wind-tunnel wall interference. To see this, consider Fig. 27, which shows the trailing vortex and its images. Initially, the vortex is displaced spanwise from the wing tip. This places vortex 1 closer to vortex image 2, having the effect of moving vortex 1 to the right. After some movement to the right, vortex 1 becomes closer to vortex image 3, and this moves vortex 1 upward. Eventually, this upward movement brings vortex 1 closer to vortex image 4, which turns vortex 1 left, back toward the wing. It should be noted that a vortex on the tunnel centerline will experience zero net cross-stream motion due to the presence of the wind-tunnel walls.

Mean Velocity Profiles

Radial profiles of tangential velocity for all blowing rates at $x/c = 0.5$ and 32 are presented in Figs. 28 and 29 respectively. In

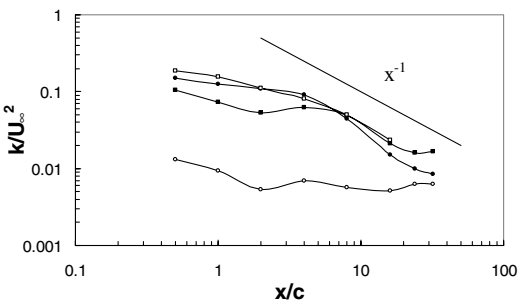

Fig. 25 Development of the turbulence kinetic energy on the vortex core. Symbols indicate $C_\mu = 0.0$ (○), 0.05 (■), 0.1 (●), and 0.28 (□).

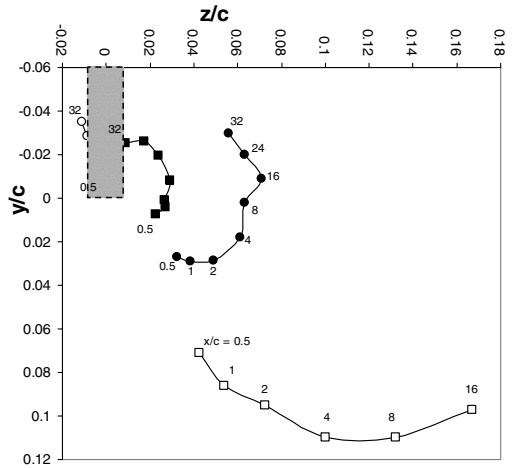

Fig. 26 Vortex core movement in the cross-stream plane. Symbols indicate $C_\mu = 0.0$ (○), 0.05 (■), 0.1 (●), and 0.28 (□). The wing silhouette is shown in gray.

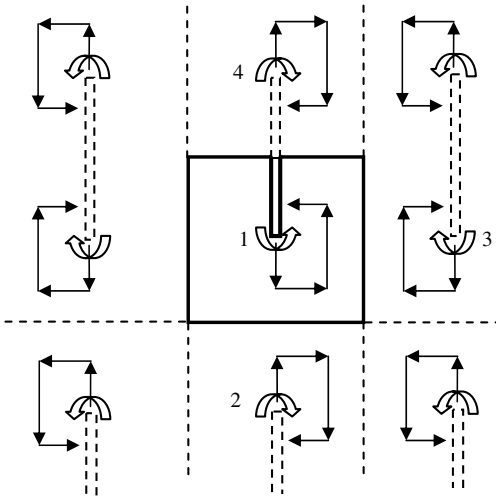

Fig. 27 Cross-stream vortex movement by images.

each case, profiles were extracted from vertical and horizontal lines passing through the center of the vortex core. As is evident in Fig. 28, the data from these horizontal and vertical sweeps expose an asymmetry that is present in the near wake. However, as the vortex develops with downstream distance, the profiles all tend toward an axisymmetric form. The theoretical tangential velocity profile given by Eq. (11) is also shown and the agreement is remarkable. Conversely, profiles based on a spatially uniform turbulent viscosity [Eq. (5)] were found to be in poor agreement with the experimental data.

Radial profiles of streamwise velocity are shown in Figs. 30 and 31. The profiles have been offset and normalized by the freestream velocity. In the near wake, the natural vortex closely fits a Gaussian form. Both cases with blowing show significant velocity surpluses that are marked by a centerline depression practically equal to the deficit of the natural vortex. With downstream distance, all velocity surpluses decline to become deficits and the profiles tend toward much the same form as a natural vortex, although the deficit with blowing is substantially less.

Circulation

Profiles of the local circulation generated from the tangential velocity profiles are shown in Figs. 32 and 33 for $x/c = 0.5$ and 32. These profiles show that blowing causes the local circulation to rise well above the freestream level. Considering the stability requirement for axisymmetric flows $d\Gamma^2/dr > 0$, these profiles are

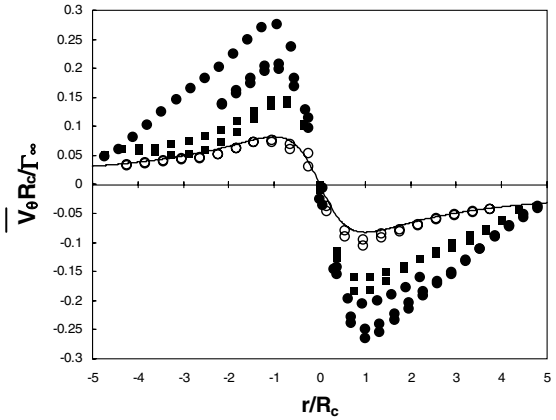

Fig. 28 Tangential velocity profiles at $x/c = 0.5$. Symbols indicate $C_\mu = 0.0$ (○), 0.05 (■), and 0.10 (●). The solid line is calculated from Eq. (11).

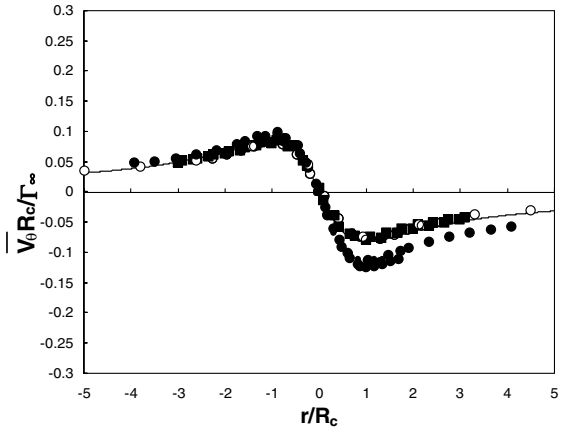

Fig. 29 Tangential velocity profiles at $x/c = 32$. Symbols indicate $C_\mu = 0.0$ (○), 0.05 (■), and 0.10 (●). The solid line is calculated from Eq. (11).

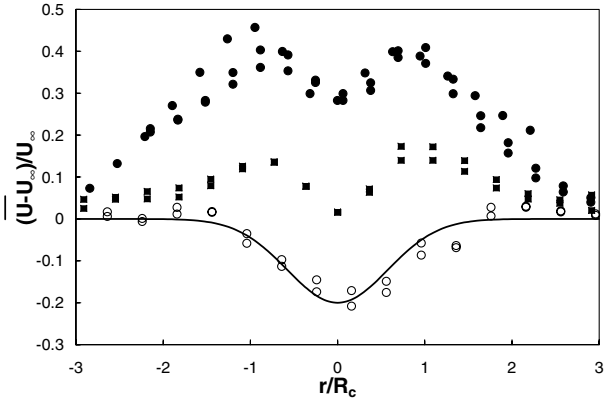

Fig. 30 Streamwise velocity profiles at $x/c = 0.5$. Symbols indicate $C_\mu = 0.0$ (○), 0.05 (■), and 0.10 (●). The solid line is a fitted Gaussian curve.

unstable and could be expected to dissipate into turbulence. At $x/c = 32$, all of the circulation profiles are tending toward the stable shape described by Uberoi [9].

Turbulence Profiles

Radial profiles of turbulence kinetic energy have been plotted in Figs. 34 and 35. The core turbulence in the near wake when using spanwise tip jets is substantially higher than the natural vortex. The

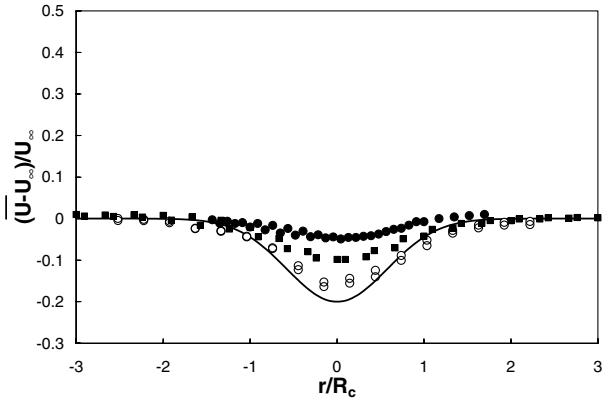

Fig. 31 Streamwise velocity profiles at $x/c = 32$. Symbols indicate $C_\mu = 0.0$ (○), 0.05 (■), and 0.10 (●). The solid line is a fitted Gaussian curve.

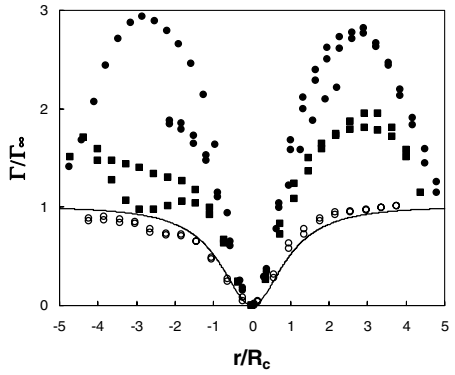

Fig. 32 Radial profiles of circulation profiles at $x/c = 0.5$. Symbols indicate $C_\mu = 0.0$ (○), 0.05 (■), and 0.10 (●). The solid line represents Eq. (11).

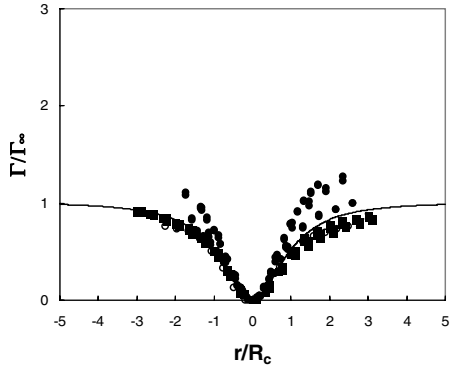

Fig. 33 Profiles of circulation at $x/c = 32$. Symbols indicate $C_\mu = 0.0$ (○), 0.05 (■), and 0.10 (●). The solid line represents Eq. (11).

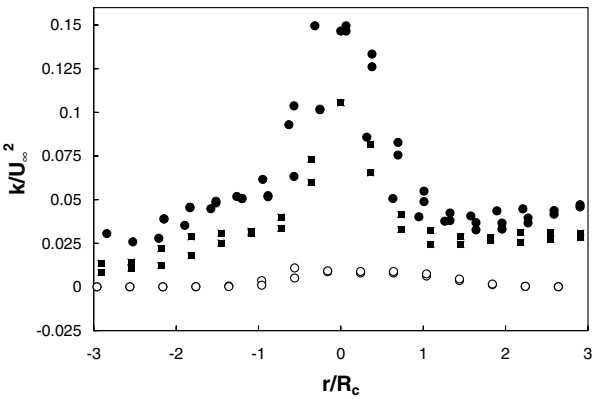

Fig. 34 Turbulence kinetic energy profiles at $x/c = 0.5$. Symbols indicate $C_\mu = 0.0$ (○), 0.05 (■), and 0.10 (●).

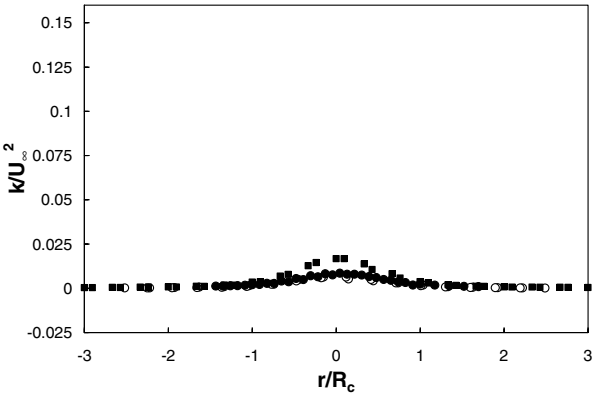

Fig. 35 Turbulence kinetic energy profiles at $x/c = 32$. Symbols indicate $C_\mu = 0.0$ (○), 0.05 (■), and 0.10 (●).

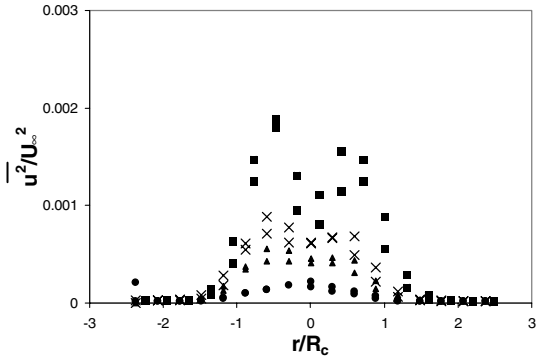

Fig. 36 Profiles of the streamwise turbulence normal stress for $C_\mu = 0.0$ at $x/c = 32$. Symbols indicate unfiltered (■), HP 10 Hz (×), HP 20 Hz (▲), and HP 100 Hz (●).

high initial turbulence levels introduced by tip blowing dissipate over the tested range and by 32 chords are comparable to the natural vortex. A noteworthy result is the remaining turbulence for the $C_\mu = 0.05$ case, even though initially lower than that for $C_\mu = 0.1$, measures higher at 32 chords downstream. This is compatible with the observation that the mean velocity gradients have greatly diminished in the $C_\mu = 0.10$ case.

A plot of the normal components of the Reynolds stresses for $C_\mu = 0.0$ at 32 chords is presented in Figs. 36–38. To evaluate the effect wandering had on these profiles, the data were high-pass filtered to various cutoff frequencies. As can be seen, the profile of $\overline{v^2}$ is by far the most affected, followed by $\overline{u^2}$ and $\overline{w^2}$. The sensitivity of the fluctuations to wandering depends to some extent on the mean velocity gradients. For example, the mean streamwise velocity is a maximum on the vortex center and has a maximum gradient at about $r/R_c = 0.5$. Thus, wandering produces double peaks in the unfiltered data of $\overline{u^2}$. The cross-stream mean velocities are a maximum at $r/R_c = 1$ and have a maximum derivative at $r/R_c = 0$. This produces central peaks in the unfiltered data of $\overline{v^2}$ and $\overline{w^2}$, as shown. The ratio of these effects suggests that the wandering motions are closely aligned (∼20 deg) with the wing span. Coincidently, double peaks in $\overline{u^2}$ are typical of wake turbulence [33]. Although not shown, the effect of filtering on the turbulence generated in flows with blowing was to give approximately the same offsets as for the natural vortex.

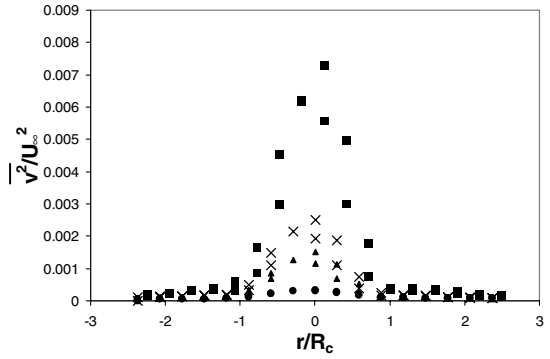

Fig. 37 Profiles of the spanwise turbulence normal stress for $C_\mu = 0.0$ at $x/c = 32$. Symbols indicate unfiltered (■), HP 10 Hz (×), HP 20 Hz (▲), and HP 100 Hz (●).

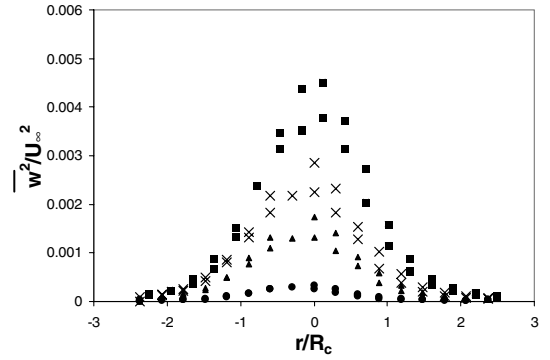

Fig. 38 Profiles of the normal stress in the direction of lift for $C_\mu = 0.0$ at $x/c = 32$. Symbols indicate unfiltered (■), HP 10 Hz (×), HP 20 Hz (▲), and HP 100 Hz (●).

Discussion

Evaluation of the Natural Vortex

There is generally good agreement between the measurements of Devenport et al. [6] and the present results for the natural vortex. The normalized tangential and streamwise velocity profiles at $x/c = 4$ and 32 from the present measurements are shown in Fig. 39. No correction has been applied for vortex wandering. For comparison, a peak value of $\bar{V}_\theta/U_\infty \approx 0.28$ was reported [6] for $x/c = 5$, although the size of the vortex core R_c in the present study is larger and has a slightly higher growth rate. The present streamwise velocity data also show a slightly larger velocity deficit in the vortex core, but the decay of the deficit is very gradual in both cases, with little change within the measurement range.

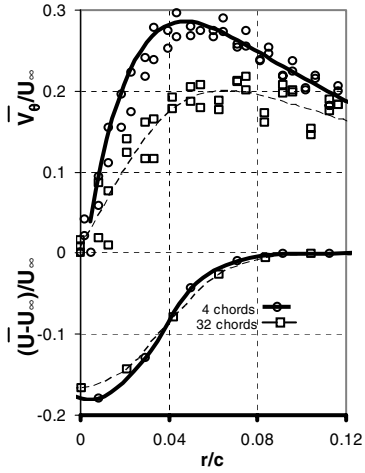

Fig. 39 Tangential and streamwise velocity profiles of the natural vortex. Solid lines represent mean values of the data. Symbols indicate $x/c = 4$ (○) and $x/c = 32$ (□).

Scaling the Turbulence Viscosity

Figure 22 shows that the rate of growth of the vortex core is strongly increased by the tip jet. Based on the assumption that the vortex core growth was due to turbulent diffusion, it was inferred that the turbulent viscosity also increases with tip jet blowing. To study this further, we may write the eddy viscosity as $\nu_T = Vl$, where the velocity scale is taken as $V = \sqrt{2k/3}$ on the vortex core and the length scale is a fraction of the core radius, $l = \beta R_c$ ($\beta < \frac{1}{2}$). The values of ν_T are taken directly from Fig. 22. A plot of $\beta = \nu_T/(R_c\sqrt{2k/3})$ is shown in Fig. 40 for all the cases considered in this study. The data appear to be divided into a group having $\beta \sim 0.05$ for $C_\mu \leq 0$ and 0.05 and $\beta > 0.15$ for $C_\mu = 0.1$ and 0.28. In the latter case, the value of β is increasing slowly with downstream distance. This dramatic change in the mixing length with blowing rate suggests a change in the structure of the turbulence in the vortex core that depends on the initial conditions set by the level of tip jet blowing. The difference is maintained throughout the measurement region.

Scaling with Wake Variables

The streamwise velocity deficit and turbulence profiles do not appear to scale with the freestream values. As an alternative scaling, consider the wake parameter $(U_c\text{-}U_\infty)$ used in Fig. 41 to reduce the mean streamwise velocity profiles to a roughly Gaussian shape.

Profiles of the kinetic energy of turbulence normalized by $(U_c\text{-}U_\infty)^2$ are shown in Fig. 42. They also show a Gaussian shape, but the profiles are not similar in these variables. This suggests that there is a substantial turbulence in the vortex core that does not scale with the mean velocity or mean velocity deficit but is residual from the initial jet or swirl flow. It should be noted that the turbulence level at 32 chords is actually higher for $C_\mu = 0.05$ than for the $C_\mu = 0.1$ case, whereas the core deficit $(U_c\text{-}U_\infty)$ for the latter is smaller.

Asymptotic Form of the Wake

In the very near wake, $x/c = 0.5$, the trailing vortices formed with tip jets contained streamwise jets and swirls in addition to highly

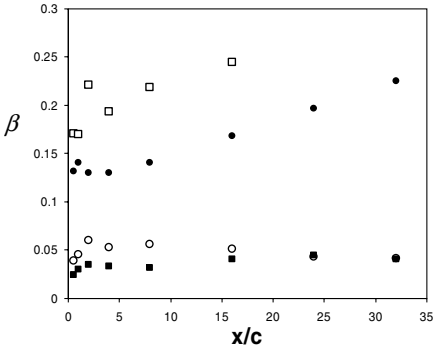

Fig. 40 Ratio of mixing length to vortex core radius. Symbols indicate $C_\mu = 0.0$ (○), 0.05 (■), 0.1 (●), and 0.28 (□).

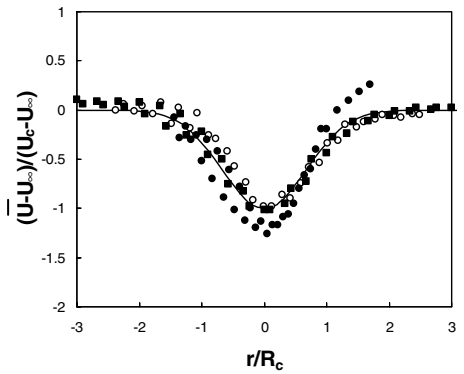

Fig. 41 Streamwise velocity deficits in wake variables at $x/c = 32$. Symbols indicate $C_\mu = 0.0$ (○), 0.05 (■), and 0.1 (●).

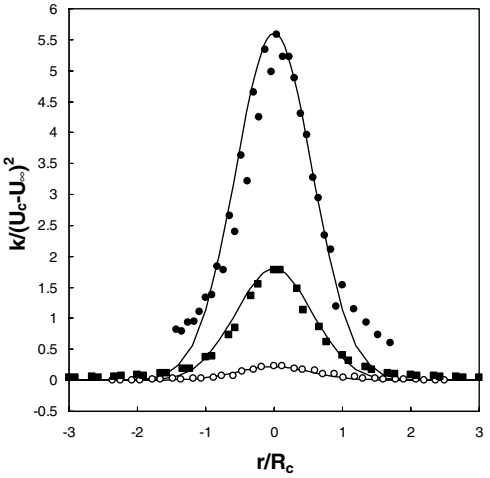

Fig. 42 Turbulence kinetic energy profiles normalized with wake deficit at $x/c = 32$. Symbols indicate $C_\mu = 0.0$ (○), 0.05 (■), and 0.1 (●).

energetic turbulence. They were generally asymmetric. In all cases, however, the velocity surplus and swirls were greatly diminished with downwind distance and by 32 chords all cases were approaching an axisymmetric form similar to the natural vortex. This is a surprising result, considering the gross distortions applied, and it suggests that all the mean motions that deviate from the residual form, closely matched by Uberoi's [9] theoretical profile, are unstable and ultimately dissipated into turbulence.

In spite of the observed profile similarity, the core size and maximum tangential velocity of the vortices at $x/c = 32$ are very different and dependent on the tip jet momentum. In effect, the application of tip jets shortened the downwind distance required for the vortex to achieve a given set of scales, R_c and $V_{\theta m} = \Gamma_\infty/2\pi R_c$. From Eq. (6), we see that the ratio of downwind distances required to achieve these scales, without and with blowing, is ν_T/ν. Referring to Fig. 22 for the case of $C_\mu = 0.1$, we have $\nu_T/\nu = 22$, at least within the range of the present measurements. Development at greater downwind distances would depend on the ultimate form of similarity that evolves for the turbulence.

Conclusions

In the near field, the spanwise tip jets added swirls and streamwise jets to the vortex core that rapidly diminished with downstream distance. They also substantially increased the rate of growth of the vortex core and the rate of decay of the maximum tangential velocity. This was especially true for $C_\mu > 0.1$.

The vortices formed both with and without tip jets had mean radial velocity profiles that approached similar axisymmetric forms within 32 chords of the trailing edge of the wing. The turbulence in the vortex core decayed rapidly with downwind distance, to levels approaching that of the natural vortex, but did not reach a state of similarity with either the tangential or streamwise mean velocity scales.

References

[1] Spalart, P. R., "Airplane Trailing Vortices," *Annual Review of Fluid Mechanics*, Vol. 30, 1998, pp. 107–38.

[2] Han, Y. O., and Leishman, J. G., "Investigation of Helicopter Rotor-Blade-Tip-Vortex Alleviation Using a Slotted Tip," *AIAA Journal*, Vol. 42, No. 3, 2004, pp. 524–535.

[3] Saffman, P. G., *Vortex Dynamics*, Cambridge Univ. Press, New York, 1992.

[4] Batchelor, G. K., "Axial Flow in Trailing Line Vortices," *Journal of Fluid Mechanics*, Vol. 20, Part 4, 1964, pp. 645–658.

[5] Brown. C. E., "Aerodynamics of Wake Vortices," *AIAA Journal*, Vol. 11, No. 4, 1973, pp. 531–536.

[6] Devenport, W. J., Rife, M. C., Liapis, S. I., and Follin, G. J., "The Structure and Development of a Wing-Tip Vortex," *Journal of Fluid Mechanics*, Vol. 312, 1996, pp. 67–106.

[7] Heyes, A. L., and Smith, D. A. R., "Spatial Perturbation of a Wing-Tip Vortex Using Pulsed Span-Wise Jets," *Experiments in Fluids*, Vol. 37, 2004, pp. 120–127.

[8] Simpson, R. G., Ahmed, N. A., and Archer, R. D., "Near Field Study of Vortex Attenuation Using Wing-Tip Blowing," *The Aeronautical Journal*, Mar. 2002, pp. 117–120.

[9] Uberoi, M. S., "Mechanisms of Decay of Laminar and Turbulent Vortices," *Journal of Fluid Mechanics*, Vol. 90, Part 2, 1979, pp. 241–255.

[10] Squire, H. B., "The Growth of a Vortex in Turbulent Flow," *Aeronautical Quarterly*, Vol. 16, Aug. 1965, pp. 302–305.

[11] Ayers, R. F., and Wilde, M. R., *An Experimental Investigation of the Aerodynamic Characteristics of a Low Aspect Ratio Swept Wing with Blowing in a Spanwise Direction from the Tips*, The College of Aeronautics, Note 57, Cranfield, England, U.K., 1956.

[12] Shi, Z., "A Study of Jets in Crossflow and Its Application on Wingtip Blowing," Doctoral Thesis, Univ. of Tennessee, Knoxville, TN, 1990.

[13] Wu, J. M., and Gilliam, F. T., "Flow Visualization Study of the Effect of Wing-Tip Jets on Wake Vortex Development," *Flow Visualization 3: Proceedings of the Third International Symposium on Flow Visualization*, Hemisphere, Washington, D.C., 1985, pp. 387–391.

[14] Wu, J. M., and Vakili, A. D., "Aerodynamic Improvements by Discrete Wingtip Jets," Flight Dynamics Lab., U.S. Air Force Wright Aeronautical Labs., Rept. WPAFWAL TR 84-3009, 1984.

[15] Wu, J. M., Vakili, A. D., and Gilliam, F. T., "Aerodynamic Interactions of Wingtip Flow with Discrete Wingtip Jets," AIAA Paper 84-2206, 1984.

[16] Wu, J. M., Vakili, A., and Chen, Z. L., "Wing-Tip Jets Aerodynamic Performance," *AIAA Aircraft Systems and Technology Conference*, AIAA, New York, 1982, pp. 1115–1121.

[17] Wu, J. M., Vakili, A. D., Chen, Z. L., and Gilliam, F. T., "Investigation on the Effects of Discrete Wingtip Jets," AIAA Paper 83-0546, 1983.

[18] Lee, C. S., Tavella, D. A., Wood, N. J., and Roberts, L., "Flow Structure of Lateral Wing-Tip Blowing," AIAA Paper 86-1810, 1986.

[19] Lee, C. S., Tavella, D. A., Wood, N. J., and Roberts, L., "Flow Structure and Scaling Laws in Lateral Wing-Tip Blowing," *AIAA Journal*, Vol. 27, No. 8, 1989, pp. 1002–1007.

[20] Tavella, D. A., Lee, C. S., and Wood, N. J., "Influence of Wing Tip Configuration on Lateral Blowing Efficiency," AIAA Paper 86-0475, 1986.

[21] Tavella, D. A., and Roberts, L., "A Theory for Lateral Wing-Tip Blowing," NASA CR-176931, 1985.

[22] Tavella, D. A., and Roberts, L., "The Concept of Lateral Blowing," AIAA Paper 85-5000, 1985.

[23] Tavella, D. A., Wood, N. J., and Harrits, P., "Measurements on Wing-Tip Blowing," NASA CR-176930, 1985.

[24] Tavella, D. A., Wood, N. J., and Harrits, P., "Influence of Tip Blowing on Rectangular Wings," AIAA Paper 85-5001, 1985.

[25] Tavella, D. A., Wood, N. J., Lee, C. S., and Roberts, L., "Two Blowing Concepts for Roll and Lateral Control of Aircraft," NASA CR-1800478, 1986.

[26] Tavella, D. A., Wood, N. J., Lee, C. S., and Roberts, L., "Lift Modulation with Lateral Wing-Tip Blowing," *Journal of Aircraft*, Vol. 25, No. 4, 1988, pp. 311–316.

[27] Jeans, T., "The Effect of Wing Tip Blowing on the Spanwise Pressure Distribution," B.S. in engineering Thesis, Univ. of New Brunswick, Fredericton, New Brunswick, Canada 2001.

[28] Bettle, J., "The Turbulent Structure of a Jet in Cross-Flow with Circulation," M.S. in engineering Thesis, Univ. of New Brunswick, Fredericton, New Brunswick, Canada 2002.

[29] Findlay, M. J., Salcudean, M., and Gartshore, I. S., "Jets in a Crossflow: Effects of Geometry and Blowing Ratio," *Journal of Fluids Engineering*, Vol. 121, June 1999, pp. 373–378.

[30] Crabbe, D., Durao, D. F. G., and Whitelaw, J. H., "A Round Jet Normal to a Crossflow," *Journal of Fluids Engineering*, Vol. 103, Mar. 1981, pp. 142–153.

[31] Andreopoulos, J., and Rodi, W., "Experimental Investigation of Jets in a Crossflow," *Journal of Fluid Mechanics*, Vol. 138, 1984, pp. 93–127.

[32] Barlow, J. B., Rae, W. H., Jr., and Pope, A., *Low-Speed Wind Tunnel Testing*, 3rd ed., Wiley, New York, 1999.

[33] Hinze, J. O., *Turbulence*, 2nd ed., McGraw–Hill, New York, 1959